Accurate Range Image Registration: Eliminating or Modelling Outliers

Li, Longzhuang; Liu, Honghai; Wei, Baogang; Liu, Yonghuai

Published in:
IEEE Conference on Emerging Technologies and Factory Automation

DOI:
10.1109/EFTA.2007.4416933

Publication date:
2007

Citation for published version (APA):
Li, L., Liu, H., Wei, B., & Liu, Y. (2007). Accurate Range Image Registration: Eliminating or Modelling Outliers. In *IEEE Conference on Emerging Technologies and Factory Automation* (pp. 1316-1323)
https://doi.org/10.1109/EFTA.2007.4416933

Accurate Range Image Registration: Eliminating or Modelling Outliers

Yonghuai Liu
Department of Computer Science
University of Wales, Aberystwyth, UK
Email: yyl@aber.ac.uk

Honghai Liu
Institute of Industrial Research
University of Portsmouth, UK
Email: Honghai.Liu@port.ac.uk

Longzhuang Li
Department of Computing Sciences
Texas A and M University, Corpus Christi, USA
Email: lli@sci.tamucc.edu

Baogang Wei
College of Computer Science
Zhejiang University, P.R. China
Email: wbg@zju.edu.cn

Abstract

Automatic and accurate range image registration is often a prerequisite step for range image analysis and interpretation. Due to occlusion, appearance and disappearance of points in different images, outliers inevitably occur. In this case, various techniques to eliminate and model outliers have been proposed for accurate range image registration. The objective of this paper is to experimentally investigate which of the outlier elimination and modelling is more effective for the evaluation of possible correspondences established, so that a deep insight into how advanced range image registration algorithms will be developed can be obtained. The experimental results based on both synthetic data and real images show that the outlier modelling often outperforms the outlier elimination in the sense of producing more accurate and robust range image registration results.

1 Introduction

The 3D imaging geometry of laser scanning systems (range cameras) creates in essence a stereo vision and/or performs some function of human brains that post-process some measures of interest and then output range images (Figure 1), depicting 3D information of the objects and environment of interest. It is likely in the future that laser scanning systems become essential components of intelligent systems due simply to the fact that the laser scanning systems directly capture depth information of the objects and environment of interest and the recovery of depth information from projective images is often sensitive to noise. The captured data are usually described in local camera centred coordinate frames. Since the laser scanning systems have limited field of view, a number of images have to be captured from different viewpoints so that a full coverage of the object surface and the environment can be obtained. To fuse the geometric and optical information in these images, they often have to be aligned into a single global coordinate frame. This process is called registration. Range image registration has two goals: one is to establish correspondences between overlapping range images, the other is to estimate the camera motion parameters that bring one range image into best possible alignment with the other. Fixing either of these two goals renders the other easier. However, they are in practice interwoven, complicating the range image registration process.

1.1 Previous work

Range image registration finds numerous applications for intelligent robots and systems such as simultaneous localization and map building (SLAM) [2]. As a result, a large number of algorithms have been developed such as techniques based on iterative closest point (ICP) [1], improved ICP algorithms [11, 13, 2], feature extraction and matching [4], genetic algorithm [12], graduated assignment algorithm [5, 9], EM-ICP [3, 6, 8], and many others.

These algorithms can be classified into three main categories with regard to automatically establishing possible correspondences: (1) feature extraction and matching (FEM) [4]; (2) closest point criterion (CPC) [1, 11, 13]; and (3) an optimal combination of points (OCP) [5, 9, 3]. Whatever method is used to establish possible correspondences between two overlapping range images, it is vital to evaluate these correspondences, since it cannot guarantee that any of these correspondences is real. Accurate evaluation of these correspondences will lead to an accurate camera motion estimation and thus range image registration. The existing methods for possible correspondence evaluation can be classified into the following four main categories or a combination of them:

1-4244-0826-1/07/$20.00 © 2007 IEEE

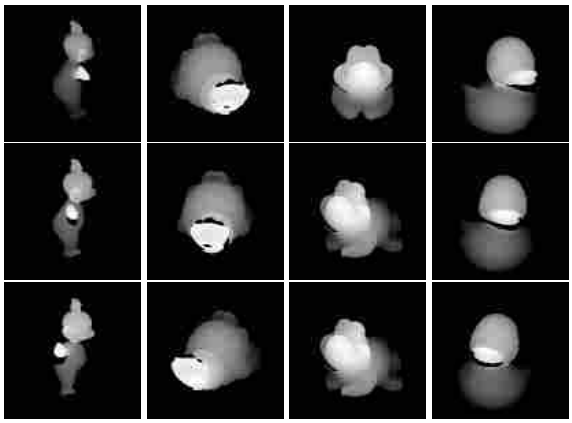

Figure 1: Real range images used. Top row: view1; Second row: view2; Bottom row: view3. From left column to right column: tubby, lobster, frog, and duck.

- Algorithms based on the information of the CPC [10]. This class of algorithms makes full use of the imaging geometry that the scanning errors occur mainly along the ray shooting from the range camera. This geometry implies that the possible correspondences must be collinear. Otherwise, it is impossible for them to represent real ones;

- Algorithms based on the information estimated from possible correspondences [7]. This class of algorithms assumes that the possible correspondences must satisfy the rigid motion constraints they were subject to. Otherwise, they cannot represent real ones. To eliminate false correspondences, the algorithms have to estimate some motion parameters of interest from the possible correspondences using the rigid motion constraints and the Monte Carlo resampling scheme;

- Algorithms based on structural constraints [13, 11]. This class of algorithms assumes that the possible correspondences must possess the same structural and optical properties. Otherwise, they cannot represent real ones. To eliminate false correspondences, the algorithms have to extract the structural constraint on, for example, the orientation of points or optical features about, for example, laser reflectance strength value of the object surface; and finally

- Algorithms based on explicit outlier modelling [5, 9, 3, 8]. This class of algorithms explicitly models outliers and thus equally treats all possible correspondences established in the sense of estimating their probabilities of being real, resulting in the camera motion parameters being estimated in the weighted least squares sense.

While the former three classes of algorithms eliminate false correspondences, the last explicitly models outliers.

1.2 Our work

The objective of this paper is to investigate which of the outlier elimination and modelling is more effective for the evaluation of the possible correspondences established, so that a deep insight into how more accurate range image registration algorithms will be developed can be obtained. The investigation is conducted through a comparative study of different algorithms that apply various strategies for the evaluation of the possible correspondences established using the traditional CPC. The reason why the possible correspondences $(\mathbf{p}_1, \mathbf{p}'_1)$ and $(\mathbf{p}_2, \mathbf{p}'_2)$ established using the traditional CPC are used is that (1) they satisfy an orientation constraint: the dot product of two vectors $\mathbf{R}(\mathbf{p}_2 - \mathbf{p}_1)$ and $\mathbf{p}'_2 - \mathbf{p}'_1$ is non-negative; (2) they satisfy a rigid distance constraint: $-1 \leq \frac{||\mathbf{p}'_2 - \mathbf{p}'_1|| - ||\mathbf{p}_2 - \mathbf{p}_1||}{||\mathbf{p}_2 - \mathbf{p}_1||} \leq \frac{2||\mathbf{R}\mathbf{p}_1 + \mathbf{t} - \mathbf{p}'_1||}{||\mathbf{p}_2 - \mathbf{p}_1||} + 1$; and (3) as long as one of the possible correspondences $(\mathbf{p}_1, \mathbf{p}'_1)$ has a limited registration error (RE) $||\mathbf{R}\mathbf{p}_1 + \mathbf{t} - \mathbf{p}'_1||$, then all others $(\mathbf{p}_2, \mathbf{p}'_2)$ must also have limited REs: $||\mathbf{p}'_2 - \mathbf{R}\mathbf{p}_2 - \mathbf{t}|| \leq ||\mathbf{R}\mathbf{p}_1 + \mathbf{t} - \mathbf{p}'_1|| + ||\mathbf{p}_2 - \mathbf{p}_1||$ where $\mathbf{R}$ and $\mathbf{t}$ are the camera motion parameters rotation matrix and translation vector respectively.

Clearly, the algorithms applicable to the evaluation of possible correspondences established using the traditional CPC are also applicable to the evaluation of possible correspondences established using either the FEM or OCP method. Choosing the former for a comparative study is because of two factors: (1) While the CPC is easier to implement, the latter is more difficult, since it involves image pre-processing for the suppression of imaging noise, feature extraction is sensitive to both imaging noise and resolution, feature matching is inherently ambiguous, and the optimization of the combination of points is not always successful; and (2) the CPC can guarantee that the established correspondences are of high quality, when compared with their neighbours, in the sense of satisfying the constraints outlined above, the quality of correspondences established using either the FEM or OCP method is unpredictable at all.

For the comparative study, four representative algorithms: collinear ICP (CICP) [10], geometric ICP (GICP) [7], Pulli pair-wise ICP (Pulli) [11], and SoftICP [9] are thus selected in this paper. Since the Pulli algorithm requires normal vector information of points which is difficult to estimate from point clouds, it will not be evaluated using synthetic data. The selected algorithms will be compared using both synthetic data with different levels of noise and sizes of overlap and real images with different sizes of camera motions and different orders and resolutions of images.

The rest of this paper is structured as follows: while Section 2 outlines the selected algorithms, Section 3 presents

the experimental results. Finally, Section 4 draws some conclusions.

2 Outline of relative algorithms

The following notations are used throughout this paper: capital letters denote vectors or matrices, lower case letters denote scalars, $|\cdot|$ denotes the absolute value of a scalar, $||\cdot||$ denotes the Euclidean norm of a vector, and superscript T denotes the transpose of a vector.

Assume that the two range images to be registered are represented as two sets of unorganised points $\mathbf{P} = \{\mathbf{p}_1, \mathbf{p}_2, \cdots, \mathbf{p}_{n_1}\}$ and $\mathbf{P}' = \{\mathbf{p}'_1, \mathbf{p}'_2, \cdots, \mathbf{p}'_{n_2}\}$, representing the same free form shape from two different nearby viewpoints with overlap in 3D space. Given that the camera motion parameters rotation matrix $\mathbf{R}$ and translation vector $\mathbf{t}$ have been initialised or estimated, the traditional ICP criterion [1] can be used to establish a set of possible correspondences $(\mathbf{p}_i, \mathbf{p}'_{c(i)})$ between $\mathbf{P}$ and $\mathbf{P}'$: $\mathbf{p}'_{c(i)} = arg\min_{\mathbf{p}' \in \mathbf{P}'} ||\mathbf{p}' - \mathbf{R}\mathbf{p}_i - \mathbf{t}||$. In order to speed up the search for the closest points $\mathbf{p}'_{c(i)}$, the optimised K-D tree data structure was employed. The selected algorithms: CICP, GICP, Pulli, and SoftICP are outlined as follows in the sense of the evaluation of these correspondences. Please refer to [10, 7, 11, 9] respectively for details.

2.1 CICP

Given a possible correspondence $(\mathbf{p}_i, \mathbf{p}'_{c(i)})$, its registration error is estimated as $e_i = ||\mathbf{p}'_{c(i)} - \mathbf{R}\mathbf{p}_i - \mathbf{t}||$ and its collinearity error is estimated as: $c_i = |\mathbf{p}'^T_{c(i)}(\mathbf{R}\mathbf{p}_i + \mathbf{t})|\ ||\frac{\mathbf{p}'_{c(i)}}{\mathbf{p}'^T_{c(i)}\mathbf{p}'_{c(i)}} - \frac{\mathbf{R}\mathbf{p}_i+\mathbf{t}}{(\mathbf{R}\mathbf{p}_i+\mathbf{t})^T(\mathbf{R}\mathbf{p}_i+\mathbf{t})}||$. Then the averages e_μ and c_μ and standard deviations e_δ and c_δ of registration errors e_i and collinearity errors c_i are computed based on those correspondences $(\mathbf{p}_i, \mathbf{p}'_{c(i)})$ where neither $\mathbf{p}_i$ nor $\mathbf{p}'_{c(i)}$ is a boundary point. Finally, the following rule is used to reject false correspondences: if $|e_i - e_\mu| < \kappa e_\delta$, $|c_i - c_\mu| < \kappa c_\delta$ and neither $\mathbf{p}_i$ nor $\mathbf{p}'_{c(i)}$ is a boundary point, then $(\mathbf{p}_i, \mathbf{p}'_{c(i)})$ is regarded as a feasible correspondence. Otherwise, it is a false one. Here κ is a parameter to be determined experimentally (generally, $\kappa \in [1.0, 1.5]$).

2.2 Geometric ICP

The GICP algorithm applies the following procedure to eliminate false correspondences:

- Use the Monte Carlo resampling method to estimate the essential point $\hat{\mathbf{e}}$ as:

$$\begin{pmatrix} (\mathbf{p}_1 - \mathbf{p}''_1)^T \\ (\mathbf{p}_2 - \mathbf{p}''_2)^T \\ (\mathbf{p}_3 - \mathbf{p}''_3)^T \\ (\mathbf{p}_4 - \mathbf{p}''_4)^T \end{pmatrix} \hat{\mathbf{e}} = \begin{pmatrix} \frac{(\mathbf{p}_1^T\mathbf{p}_1 - \mathbf{p}''^T_1\mathbf{p}''_1)}{2} \\ \frac{(\mathbf{p}_2^T\mathbf{p}_2 - \mathbf{p}''^T_2\mathbf{p}''_2)}{2} \\ \frac{(\mathbf{p}_3^T\mathbf{p}_3 - \mathbf{p}''^T_3\mathbf{p}''_3)}{2} \\ \frac{(\mathbf{p}_4^T\mathbf{p}_4 - \mathbf{p}''^T_4\mathbf{p}''_4)}{2} \end{pmatrix}$$

  where $(\mathbf{p}_i, \mathbf{p}''_i) = (\mathbf{p}_i, -\mathbf{p}'_{c(i)})$ $(i = 1, 2, 3, 4)$ are any four possible reflected correspondences. This is a linear equation group which can be solved using the total least squares method;

- Compute the relative gaps of each possible reflected correspondence $(\mathbf{p}_i, \mathbf{p}''_i)$:

$$\gamma_{1\,i} = \frac{|\ ||\mathbf{p}_i - \hat{\mathbf{e}}|| - ||\mathbf{p}''_i - \hat{\mathbf{e}}||\ |}{\max(||\mathbf{p}_i - \hat{\mathbf{e}}||, ||\mathbf{p}''_i - \hat{\mathbf{e}}||)}$$
$$\gamma_{2\,i} = \frac{|\ ||\underline{\mathbf{p}_i} - \underline{\hat{\mathbf{e}}}|| - ||\underline{\mathbf{p}''_i} - \underline{\hat{\mathbf{e}}}||\ |}{\max(||\underline{\mathbf{p}_i} - \underline{\hat{\mathbf{e}}}||, ||\underline{\mathbf{p}''_i} - \underline{\hat{\mathbf{e}}}||)}$$

  where $\underline{\mathbf{p}_i} = (\mathbf{I} - \mathbf{h}\mathbf{h}^T)\mathbf{p}_i$, $\underline{\mathbf{p}''_i} = (\mathbf{I} - \mathbf{h}\mathbf{h}^T)\mathbf{p}''_i$, $\underline{\hat{\mathbf{e}}} = (\mathbf{I} - \mathbf{h}\mathbf{h}^T)\hat{\mathbf{e}}$, and $\mathbf{h}$ is the estimated rotation axis of the camera motion at the previous iteration. The candidates to $\hat{\mathbf{e}}$ are finally synthesized using the median filter;

- Compute the mean μ and standard deviation σ of the gaps:

$$\mu_{\gamma_1} = \frac{1}{n_1}\sum_{i=1}^{n_1}\gamma_{1\,i},\ \ \sigma_{\gamma_1} = \sqrt{\frac{1}{n_1}\sum_{i=1}^{n_1}(\gamma_{1\,i} - \mu_{\gamma_1})^2}$$
$$\mu_{\gamma_2} = \frac{1}{n_1}\sum_{i=1}^{n_1}\gamma_{2\,i},\ \ \sigma_{\gamma_2} = \sqrt{\frac{1}{n_1}\sum_{i=1}^{n_1}(\gamma_{2\,i} - \mu_{\gamma_2})^2}$$

- Eliminate possible false correspondences: If $|\gamma_{1\,i} - \mu_{\gamma_1}| > \sigma_{\gamma_1}$ or $|\gamma_{2\,i} - \mu_{\gamma_2}| > \sigma_{\gamma_2}$, then the possible correspondence $(\mathbf{p}_i, \mathbf{p}'_{c(i)})$ is regarded as a false one.

2.3 Pulli ICP

Any possible correspondence $(\mathbf{p}_i, \mathbf{p}'_{c(i)})$ cannot be real if: (1) either $\mathbf{p}_i$ or $\mathbf{p}'_{c(i)}$ is a boundary point, (2) the including angle between the normals at $\mathbf{R}\mathbf{p}_i$ and $\mathbf{p}'_{c(i)}$ is larger than $45°$, (3) the distance between $\mathbf{R}\mathbf{p}_i + \mathbf{t}$ and $\mathbf{p}'_{c(i)}$ is larger than a threshold, which was determined as four times the resolution of the range images to be registered, and (4) it is ranked into the worst 10% among all possible correspondences according to their registration errors $||\mathbf{R}\mathbf{p}_i + \mathbf{t} - \mathbf{p}'_{c(i)}||$.

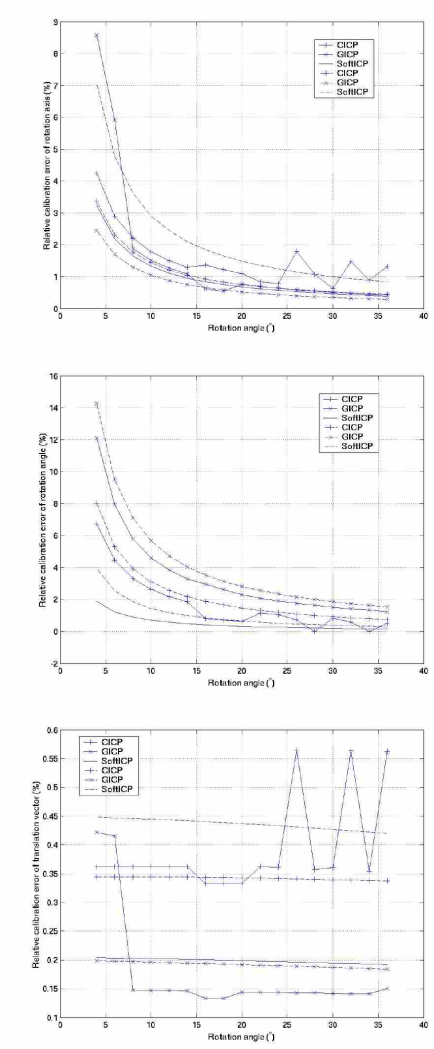

Figure 2: The relationship between the parameters of interest and the rotation angle. Top: rotation axis; Middle: rotation angle; Bottom: translation vector.

2.4 SoftICP

The following SoftICP algorithm is proposed in [9, 8] for automatic 3D free form shape matching:

Initialize $\mathbf{R}$ to the identity matrix, $\mathbf{t}$, β to β_0, $\hat{m}_i$ to $1/n_1$

Begin A: Do A until ($\beta \geq \beta_f$)

Begin B: Do B until the relative variations of both rotational and translational vectors at successive two iterations are larger than a threshold ρ or # of iterations $> I_0$

Use the ICP criterion [1] to establish a set of possible correspondences $(\mathbf{p}_i, \mathbf{p}'_{c(i)})$ between $\mathbf{P}$ and $\mathbf{P}'$;

Begin C (**update correspondence parameters by SoftAssign**):

Compute the corresponding matching error Q as:

$$Q_{i1} = ||\mathbf{p}'_{c_{(i)}} - \mathbf{R}\mathbf{p}_i - \mathbf{t}||^2 \ (i = 1, 2, \cdots, n_1),$$
$$Q_{i2} = ||\mathbf{p}'_{n_2+1} - \mathbf{R}\mathbf{p}_i - \mathbf{t}||^2 \ (i = 1, 2, \cdots, n_1),$$
$$Q_{n_1+1j} = ||\mathbf{p}'_j - \mathbf{R}\mathbf{p}_{n_1+1} - \mathbf{t}||^2 \ (j = 1, 2, \cdots, n_2).$$

Compute the ragged matching array $\mathbf{M}$ as:

$$m_{i1} = exp(-\beta(Q_{i1} - \alpha)) \ (i = 1, 2, \cdots, n_1),$$
$$m_{i2} = exp(-\beta_0(Q_{i2} - \alpha)) \ (i = 1, 2, \cdots, n_1),$$
$$m_{n_1+1j} = exp(-\beta_0(Q_{n_1+1j} - \alpha)) \ (j = 1, 2, \cdots, n_2).$$

Begin E: Impose the two-way constraint

For each row i ($i = 1, 2, \cdots, n_1$), the normalisation is implemented as: $\hat{m}^1_{ij} \leftarrow \frac{\hat{m}^0_{ij}}{\sum_{j=1}^{j=2} \hat{m}^0_{ij}}$ (j=1, 2);

Initialise the sum of matching probabilities for each point in $\mathbf{P}'$ as: $s(j) = \hat{m}^1_{n_1+1j}$ $(j = 1, 2, \cdots, n_2)$;

Consider the matching probability for any point in $\mathbf{P}'$ found as a possible point correspondent by a point in $\mathbf{P}$: $s(c(i)) \leftarrow s(c(i)) + \hat{m}^1_{i1}$ $(i = 1, 2, \cdots, n_1)$;

Normalise each column (with sparse elements) in $\mathbf{M}$ as: $\hat{m}^0_{i1} = \frac{\hat{m}^1_{i1}}{s(c(i))}$ $(i = 1, 2, \cdots, n_1)$, $\hat{m}^0_{n_1+1j} = \frac{\hat{m}^1_{n_1+1j}}{s(j)}$ $(j = 1, 2, \cdots, n_2)$;

End E

End C

Begin D (**update camera motion parameters using** the **quaternion method**)

Update $\mathbf{R}$, $\mathbf{t}$ from the objective function: $E_{3D}(\mathbf{R}, \mathbf{t}) = \min_{\mathbf{R},\mathbf{t}} \sum_{i=1}^{n_1} m_{i1} ||\mathbf{p}'_{c(i)} - \mathbf{R}\mathbf{p}_i - \mathbf{t}||^2$

End D

End B

$\beta \leftarrow \beta_r \beta$

End A

where β_0 denotes the initial inverse temperature for deterministic annealing, β_r the inverse temperature increasing rate, β_f the final inverse temperature, α is the squared registration error of a real correspondence, ρ is the expected relative camera motion estimation error, I_0 is the maximum iteration number, and $\mathbf{p}_{n_1+1}$ and $\mathbf{p}'_{n_2+1}$ are slack variables for the explicit outlier modelling.

3 Experimental results

In this section, we compare four state of the art ICP variants CICP [10], GICP [7], Pulli pair-wise ICP [11] and the SoftICP algorithm [9, 8] for the evaluation of possible correspondences based on both synthetic data and real images. All experiments were implemented on a Pentium IV, 2.80GHz computer.

Table 1: The average μ and standard deviation σ of the relative calibration errors $e_{\mathbf{h}}$, e_θ, and $e_{\mathbf{t}}$ in percentage of rotation axis $\hat{\mathbf{h}}$, rotation angle $\hat{\theta}$, and translation vector $\hat{\mathbf{t}}$ using synthetic data corrupted by different levels of noise.

Noise	Measure	Method	$e_{\mathbf{h}}(\%)$	$e_\theta(\%)$	$e_{\mathbf{t}}(\%)$
σ_1	μ	CICP	1.55	1.66	0.39
		GICP	1.56	4.43	0.17
		SoftICP	0.98	0.50	0.20
	σ	CICP	0.86	1.72	0.08
		GICP	2.16	2.79	0.09
		SoftICP	0.74	0.45	0.00
σ_2	μ	CICP	1.06	2.24	0.34
		GICP	0.75	4.16	0.19
		SoftICP	2.14	1.03	0.43
	σ	CICP	0.76	1.89	0.00
		GICP	0.56	3.29	0.00
		SoftICP	1.61	0.94	0.01

3.1 Synthetic data with sparse points

First n points $\mathbf{P} = \{\mathbf{p}_1, \mathbf{p}_2, \cdots, \mathbf{p}_n\}$ were randomly generated with uniform distribution within the 3D space $[10, 20] \times [10, 20] \times [10, 20]$. These points were then subjected to a rotation angle θ around a fixed rotation axis $\mathbf{h}$ (subject to normalization) randomly generated with uniform distribution within the 3D space $[1, 3] \times [1, 3] \times [1, 3]$ followed by a constant translation vector $\mathbf{t}$ randomly generated with uniform distribution within the 3D space $[10, 20] \times [10, 20] \times [10, 20]$. Let the transformed points be $\mathbf{P'} = \{\mathbf{p}'_1, \mathbf{p}'_2, \cdots, \mathbf{p}'_n\}$. Once the data were generated we thus, have precise knowledge of the selected points and their correspondents $(\mathbf{p}_i, \mathbf{p}'_i)(i = 1, 2, \cdots, n)$ and motion parameters rotation matrix $\mathbf{R}$ and translation vector $\mathbf{t}$ to serve as reference for error estimation and validation of the algorithms.

In order to simulate real world noise contaminated data, Gaussian white noise was added to the coordinates of each point with standard deviation $\sigma_1 = 0.04$ in one series of experiments and $\sigma_2 = 0.08$ in another. In order to simulate occlusion and appearance and disappearance of points, unless otherwise stated, we removed the last 25% points in $\mathbf{P}$ and the first 15% points in $\mathbf{P'}$. Finally we obtained two new sets of points $\mathbf{P}$ and $\mathbf{P'}$ for registration with 60% overlap in 3D space. The parameters of interest are the relative estimation errors of rotation axis $\hat{\mathbf{h}}$, rotation angle $\hat{\theta}$ and translation vector $\hat{\mathbf{t}}$ of the camera motion.

3.1.1 Different levels of noise

In this section, we do a comparative study of performance of different algorithms for the evaluation of possible correspondences using data that were corrupted by different levels of Gaussian white noise. The experimental results are presented in Figure 2 and Table 1 (n=100). In the figure, the solid lines correspond to the low level σ_1 of noise, the dash lines correspond to the high level σ_2 of noise, lines with pluses correspond to the CICP algorithm, lines with crosses correspond to the GICP algorithm, and lines without any signs correspond to the SoftICP algorithm.

From Figure 2, it can be seen that while both the CICP and GICP algorithms are significantly less accurate than the SoftICP algorithm, the former is not stable. This is because the CICP algorithm has to determine the parameter κ to reject false correspondences which is dependent on the camera motion, the distribution of the data points and the size of overlap between the data sets to be registered. In contrast, the SoftICP algorithm uniformly treats all possible correspondences in the sense of estimating their probabilities of being real embedded into the powerful deterministic

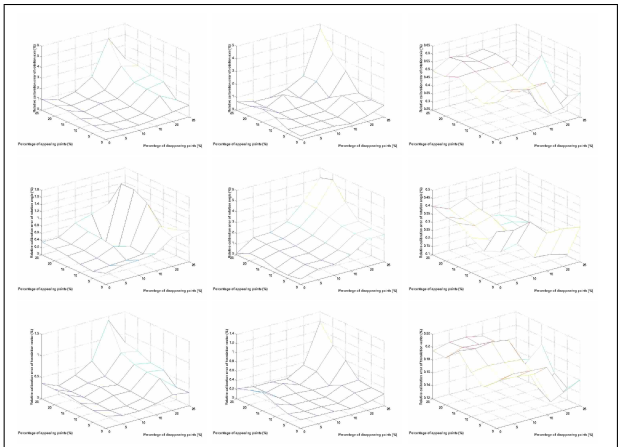

Figure 3: The relationship between the parameters of interest and the percentages of disappearing and appearing points in different data sets. Top row: rotation axis; Middle row: rotation angle; Bottom row: translation vector. Left column: CICP; Middle column: GICP; Right column: SoftICP.

Table 2: The average μ and standard deviation σ of the relative calibration errors $e_{\mathbf{h}}$, e_θ, and $e_{\mathbf{t}}$ in percentage of rotation axis $\hat{\mathbf{h}}$, rotation angle $\hat{\theta}$, and translation vector $\hat{\mathbf{t}}$ using synthetic data corrupted by different levels of noise.

Measure	Method	$e_{\mathbf{h}}(\%)$	$e_\theta(\%)$	$e_{\mathbf{t}}(\%)$
μ	CICP	1.27	0.59	0.40
	GICP	0.80	1.78	0.26
	SoftICP	0.46	0.28	0.20
σ	CICP	0.95	0.41	0.25
	GICP	0.88	1.24	0.21
	SoftICP	0.08	0.09	0.02

annealing scheme, leading the camera motion parameters to be accurately estimated in the weighted least squares sense, instead of in the least squares sense.

3.1.2 Different percentages of appearing and disappearing points

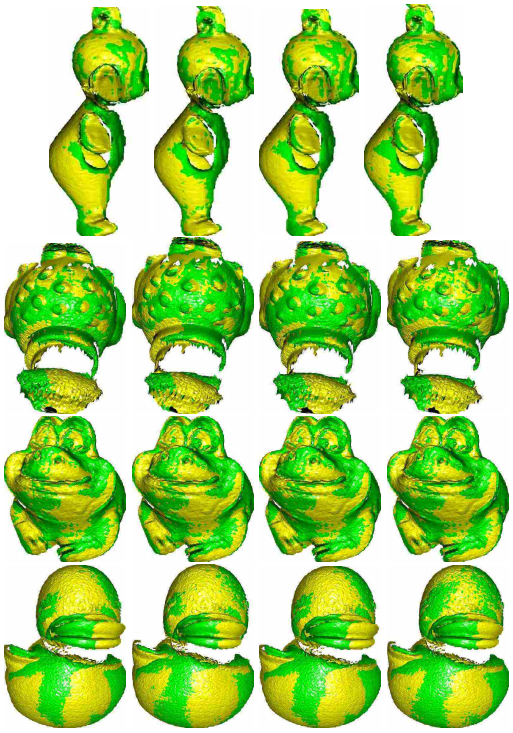

Figure 4: Final registration results of images subject to small motions. Left column: CICP; Second column: GICP; Third column: Pulli; Right column: SoftICP. Top row: tubby1-2; Second row: lobster1-2; Third row: frog1-2; Bottom row: duck1-2.

In this section, we report the experimental results about the sensitivity of different algorithms to the appearance and disappearance of points in different data sets. The rotation angle of the camera motion was fixed: $\theta = 25°$. The experimental results are presented in Figure 3 and Table 2.

From Figure 3, it can be seen that while the SoftICP algorithm produced relatively stable results, both the CICP and GICP algorithms perform worse with the percentages of appearing and disappearing points increasing. This is because more disappearing and appearing points imply that more outliers will be generated by the traditional CPC. In this case, the setting of the parameter κ as a constant in the CICP algorithm does not reflect the percentage of actual overlap between two point sets being registered. A large number of outliers renders the Monte Carlo resampling scheme the GICP algorithm to degrade for the estimation of the essential point $\hat{\mathbf{e}}$, resulting in an incomplete elimination of false correspondences.

3.2 Real images with dense points

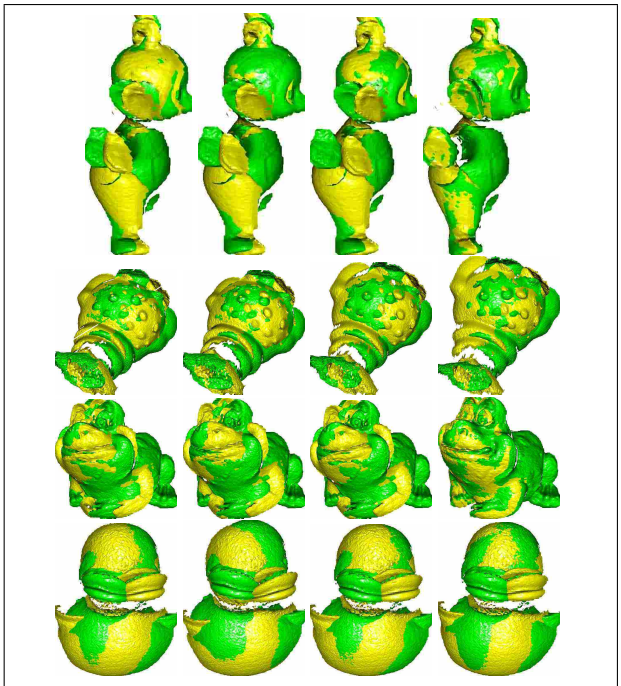

Figure 5: Final registration results of images subject to large motions. Left column: CICP; Second column: GICP; Third column: Pilli; Right column: SoftICP. Top row: tubby1-3; Second row: lobster1-3; Third row: frog1-3; Bottom row: duck-3.

In this section, we report the experimental results based on real images. The real range images (Figure 1) used in this paper were downloaded from a publicly available range image database currently hosted by the Signal Analysis and Machine Perception laboratory at Ohio State University, were captured using a Minolta Vivid 700 range camera, and are of the same size of 200×200 pixels. The parameters of interest are the average and standard deviation of registration errors of the reciprocal correspondences (RCs), the estimated rotation angles of the camera motions that can be derived from the image file name encoding, and the time for registration. In Figures 4 and 5, yellow colour represents the transformed first images, the green colour represents the second images.

3.2.1 Small motions

Since the ICP algorithm requires a good initialisation of camera motion parameters, in this section, we report the

Table 3: The average e_μ and standard deviation e_δ of registration errors in millimetres based on RCs, expected rotation angle θ and calibrated rotation angle $\hat{\theta}$ in degrees, the number N of finally established RCs, and registration time t in seconds for different algorithms applied to different range images.

Image	q	e_μ (mm)	e_δ (mm)	θ $(^\circ)$	$\hat{\theta}$ $(^\circ)$	N	t (s)
tubby1-2	CICP	0.28	0.15	20	18.80	3140	10
	GICP	0.26	0.15		19.66	3092	9
	Pulli	0.27	0.15		19.14	3140	16
	SoftICP	0.27	0.15		19.35	3134	16
lobster1-2	CICP	0.45	0.32	20	17.96	4469	17
	GICP	0.44	0.36		20.94	4320	16
	Pulli	0.45	0.32		17.77	4498	53
	SoftICP	0.42	0.32		18.12	4617	34
frog1-2	CICP	0.30	0.30	20	18.48	5304	14
	GICP	0.29	0.30		18.90	5304	18
	Pulli	0.29	0.30		18.72	5313	49
	SoftICP	0.29	0.30		19.11	5343	29
duck1-2	CICP	0.42	0.26	20	6.81	6931	19
	GICP	0.35	0.20		13.20	7147	19
	Pulli	0.41	0.25		7.56	6951	79
	SoftICP	0.36	0.23		11.55	7137	40

Table 4: The average e_μ and standard deviation e_δ of registration errors in millimetres based on RCs, expected rotation angle θ and calibrated rotation angle $\hat{\theta}$ in degrees, the number N of finally established RCs, and registration time t in seconds for different algorithms applied to different range images.

Image	q	e_μ (mm)	e_δ (mm)	θ $(^\circ)$	$\hat{\theta}$ $(^\circ)$	N	t (s)
tubby1-3	CICP	0.54	0.33	40	28.61	1717	15
	GICP	0.51	0.31		26.92	1708	13
	Pulli	0.52	0.33		19.96	1771	19
	SoftICP	0.26	0.19		39.29	2068	35
lobster1-3	CICP	0.69	0.54	40	58.90	2660	37
	GICP	0.65	0.49		54.34	2653	31
	Pulli	0.70	0.52		58.00	2609	92
	SoftICP	0.63	0.60		68.91	2665	69
frog1-3	CICP	0.47	0.49	40	26.46	2389	25
	GICP	0.50	0.36		23.96	2193	28
	Pulli	0.49	0.32		26.05	2244	54
	SoftICP	0.33	0.28		38.15	3199	38
duck1-3	CICP	0.59	0.42	40	9.13	5108	30
	GICP	0.64	0.47		14.02	4676	32
	Pulli	0.59	0.43		8.57	5167	86
	SoftICP	0.51	0.38		9.09	5349	59

experimental results for the automatic registration of overlapping range images subject to relatively small motions. Doing so provides an ideal condition for all algorithms to register overlapping range images. The experimental results are presented in Figure 4 and Table 3.

From Figure 4, it can be seen that while all algorithms accurately register both the tubby and lobster images, they inaccurately register the duck images, especially the CICP and Pulli algorithms displace the wings of duck in the two images. This conclusion has been clearly confirmed by the smaller rotation angles of the camera motion estimated in Table 3. Due to the necessity to do the statistics on the average distance between neighbouring points in images being registered, the Pulli algorithm generally takes longer time for registration.

3.2.2 Large motions

In this section, we report the experimental results for the automatic registration of overlapping range images subject to relatively large motions with rotation angles as large as 40°. Since large motions violate the assumption of the ICP algorithm, it is expected that all the ICP variants will perform poorly. The experimental results are presented in Figure 5 and Table 4.

From Figure 5 and Table 4, it can be seen that there is a large variation among the registration results. While the CICP, GICP, and Pulli algorithms all displace the hands and ears of tubby in the images and the mouths and front legs of frog in the images, the SoftICP algorithm accurately registered all of them. When the range images are of low quality, as is the case for both the lobster and duck images, all algorithms performed poorly. This shows that more accurate and stable algorithms still need to be developed.

Table 5: The average e_μ and standard deviation e_δ of registration errors in millimetres based on RCs, expected rotation angle θ and calibrated rotation angle $\hat{\theta}$ in degrees, and registration time t in seconds for different algorithms applied to different range images.

Image	Algo.	$e_\mu(mm)$	$e_\delta(mm)$	$\theta(^\circ)$	$\hat{\theta}(^\circ)$	$t(s)$
tubby3-1	CICP	0.45	0.26	40	32.74	16
	GICP	0.44	0.26		32.03	13
	Pulli	0.40	0.25		25.95	20
	SoftICP	0.25	0.19		39.44	32
lobster3-1	CICP	0.67	0.51	40	57.80	30
	GICP	0.51	0.38		41.85	22
	Pulli	0.67	0.47		55.86	89
	SoftICP	0.63	0.63		67.79	59
frog3-1	CICP	0.66	0.53	40	26.39	43
	GICP	0.66	0.53		43.79	27
	Pulli	0.66	0.54		39.19	84
	SoftICP	0.55	0.49		46.56	81
duck3-1	CICP	0.53	0.36	40	10.87	31
	GICP	0.56	0.37		10.57	32
	Pulli	0.55	0.38		9.93	78
	SoftICP	0.48	0.35		15.24	52

3.2.3 Image order

In this section, we reverse the image orders so that we can test whether algorithms will produce different results. The experimental results are presented in Table 5.

Table 5 shows that quite different results have been produced in the sense of average registration error and the rotation angle of the camera motion. While the SoftICP algorithm still accurately registers the tubby images, the GICP algorithm produces a difference in the rotation angle of the camera motion of as large as 20° for the registration of the frog images. This shows that image orders do have a subtle effect on the performance of the ICP algorithms.

Table 6: The average e_μ and standard deviation e_δ of registration errors in millimetres based on RCs, expected rotation angle θ and calibrated rotation angle $\hat{\theta}$ in degrees, and registration time t in seconds for different algorithms applied to different range images.

Image	q	$e_\mu(mm)$	$e_\delta(mm)$	$\theta(^\circ)$	$\hat{\theta}(^\circ)$	$t(s)$
tubby1-3	CICP	0.75	0.40	40	27.66	11
	GICP	0.74	0.42		26.34	11
	Pulli	0.84	0.50		5.43	9
	SoftICP	0.46	0.20		38.73	14
lobster1-3	CICP	1.03	0.61	40	60.39	14
	GICP	0.95	0.54		52.98	11
	Pulli	1.02	0.67		37.55	12
	SoftICP	1.01	0.78		68.75	16
frog1-3	CICP	0.73	0.38	40	25.16	12
	GICP	0.73	0.38		25.58	13
	Pulli	0.76	0.41		24.26	13
	SoftICP	0.53	0.48		37.88	13
duck1-3	CICP	0.83	0.47	40	9.14	11
	GICP	0.91	0.60		13.21	12
	Pulli	0.83	0.47		9.23	13
	SoftICP	0.76	0.45		8.59	15

3.2.4 Image resolution

In this section, we test different algorithms using low resolution images. Low resolution images were generated using the uniform sampling: odd pixels in each row in the original raster file. The experimental results are presented in Table 6.

Table 6 shows that except the fact that all algorithms have produced larger average registration errors, as expected, the Pulli algorithm produced a variation in the rotation angle of the camera motion of as large as 15° for the registration of the tubby and lobster images. This shows that image resolutions also have a subtle effect on the registration results of the ICP algorithms.

4 Conclusions

In this paper, we have compared four representative ICP variants using both synthetic data and real images with an attempt to reveal which of the outlier elimination and modelling is more effective for the evaluation of the possible correspondences established. The experimental results show: (1) the image quality is vital for accurate range image registration. This means that the images must be complex enough to deliver the camera motion information. Poor quality images like lobster and duck will present a challenge to any algorithm for registration and registration errors easily crop up; (2) The SoftICP algorithm usually produces the smallest average registration errors. This shows that the explicit outlier modelling often outperforms the outlier elimination in the sense of achieving accurate automatic range image registration results, since the classification of possible correspondences into either real or false ones is not always successful, due to the fact that the classification is often data dependent; and (3) While the SoftICP algorithm often produces better registration results, it is often more computationally expensive, since it adopts the iterative deterministic annealing scheme for the optimization of the probabilities of the possible correspondences established. Further research is to accurately model outliers for automatic range image registration in the process of underwater oil pipe modelling and inspection. Research is under way and the results will be reported in the future.

References

[1] P. J. Besl, N. D. McKay. A method for registration of 3D shapes. *IEEE Trans. PAMI*, 14(1992) 239-256.

[2] D.M. Cole and P.M. Newman. Using laser range data for 3D SLAM in outdoor environments. *Proc. ICRA*, 2006, pp. 188-193.

[3] G. Dewaele, F. Devernay, and H. Horaud. Hand motion from 3D point trajectories and a smooth surface model. *Proc. ECCV*, 2004, pp. 495-507.

[4] H.Q. Dinh, S. Kropac. Multi-resolution spin images. *Proc. CVPR*, 2006, pp. 863-870.

[5] S. Gold, A. Rangarajan, et al. New algorithms for 2-D and 3-D point matching: pose estimation and correspondence. *Pattern Recognition* 31(1998) 1019-1031.

[6] S. Granger and Xavier Pennec, Multi-scale EMICP: a fact and robust approach for surface registration, *Proc. ECCV*, 2002, LNCS, pp. 418-432.

[7] Y. Liu, M.A. Rodrigues, and Y. Wang. Developing rigid motion constraints for the registration of free-form shapes. *Proc. IEEE/RSJ IROS*, 2000, pp. 2280-2285.

[8] Y. Liu. Automatic registration of overlapping 3D point clouds using closest points. *Image and Vision Computing*, 24(2006) 762-781.

[9] Y. Liu. Automatic 3d free form shape matching using the graduated assignment algorithm. *Pattern Recognition*, 38(2005) 1615-1631.

[10] Y. Liu, L. Li, B. Wei. 3D shape matching using collinearity constraint. *Proc. ICRA*, 2004, pp. 2285-2290.

[11] K. Pulli. Multiview registration for large data sets. *Proc. 3DIM*, 1999, pp. 160-168.

[12] L. Silva, Olga R.P. Bellon, and K.L. Boyer. Precision range image registration using a robust surface interpenetration measure and enhanced genetic algorithms. *IEEE Trans. PAMI*, 27(2005) 762-776.

[13] G. Turk and M. Levoy. Zippered polygon meshes from range images. *Proc. SIGGRAPH*, pp. 311-318, 1994.